Near-Infrared Light Scattering by Terrestrial Clouds

JAMES E. HANSEN

Goddard Institute for Space Studies, NASA, New York, N. Y.

AND JAMES B. POLLACK

Center for Radiophysics and Space Research, Cornell University, Ithaca

(Manuscript received 22 September 1969, in revised form 12 December 1969)

ABSTRACT

Calculations of the reflectivity of water clouds (liquid and ice particles) are compared to observations of terrestrial clouds in the near infrared. The presentation is divided into four parts which may be consulted individually. Section 3 presents new Mie scattering calculations of general interest, Sections 4–7 compare multiple-scattering results to cloud observations, Section 8 suggests a revision in the optical constants of ice for $\lambda \approx 3\ \mu$, and the Appendix details several methods which substantially reduce the work load in multiple-scattering computations.

Our results indicate that it is possible to use the spectral variation of the reflectivity to derive the size of the cloud particles and their phase (liquid or solid) as well as the total optical depth of the clouds. Typical results show dense cirrus clouds to have an optical depth ≥ 10 and to be composed of ice particles of mean radius 15–20 μ; the cumulus clouds which were analyzed showed a more variable, but usually smaller, particle size.

In spectral regions where the single-scattering albedo is high it is found that most of the gas absorption takes place within the clouds rather than above them.

1. Introduction

Sagan and Pollack (1967), Pollack and Sagan (1968), and Hansen and Cheyney (1968, 1969) have pointed out that some physical properties of clouds, such as mean particle size and optical depth, can be inferred from an analysis of the clouds' near-infrared reflectivity. Below we analyze observations of terrestrial water and ice clouds with this expectation in mind. It affords us an opportunity both to deduce the properties of these clouds and to check the consistency of our approach when applied to clouds we know something about. It is especially important to obtain tests of the plane-parallel approximation for real atmospheric cloud systems and the Mie scattering approximation for ice crystals.

After outlining our computational scheme, we summarize the theoretical results for single scattering. These illustrate the effects on the scattering of various input parameters. Subsequently, we discuss the infrared observations of Blau *et al.* and attempt to remove the effects of gaseous absorption. In the next section we summarize the absorption corrections and relate them to the clouds' temperature and to the mode of line formation. Finally, we estimate the phase, mean particle size, and optical depth of selected clouds from their spectral and angular scattering behavior.

2. Computational method

To obtain the spectral reflectivity of clouds and the angular distribution of the scattered light we first computed the single scattering from a small volume containing a representative distribution of particle sizes and then the multiple scattering for the entire cloud. The single-scattering computations were made using the Mie theory in essentially the way described by Deirmendjian and Clasen (1962). However, the logarithmic derivatives of certain spherical Bessel functions occurring in the series were obtained by proceeding from the highest order terms; Kattawar and Plass (1967) have pointed out that an upward progression for the recursion relations is basically unstable and may cause significant errors for large size parameters. The validity of our single-scattering solutions was checked by making comparisons to published results of Deirmendjian (1964), unpublished company reports by the same author, and unpublished work of H. Cheyney.

We employed Deirmendjian's (1964) "cloud model" for the distribution of particle sizes, i.e.,

$$n(r) \propto r^6 \exp(-6r/r_m), \tag{1}$$

where $n(r)$ is the volume concentration of radius r, and r_m is the radius at which the distribution has its maximum. Although sample size distributions from actual

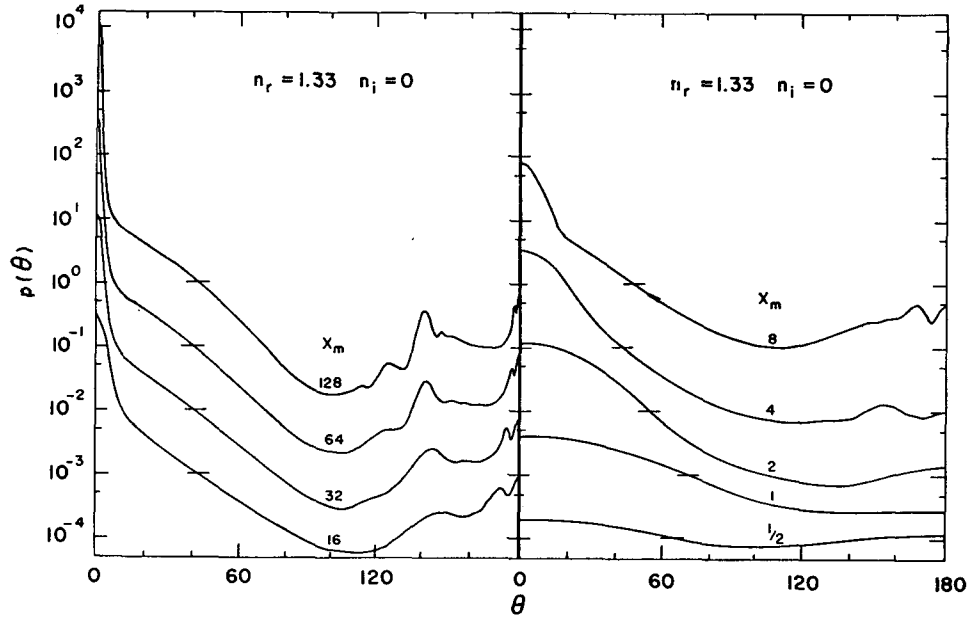

FIG. 1. Single-scattering phase functions for a size distribution of transparent spherical particles with a real refractive index typical of water and ice in the near infrared; the curves show the effect of changing the characteristic particle size. In Figs. 1–3 the vertical scales apply to the uppermost curve on the left side and the scales for the other curves may be obtained by multiplication by a power of 10 such that the horizontal bar on each curve occurs at $p(\theta) = 1$.

clouds often differ markedly from Deirmendjian's model, it serves the purpose of averaging out most of the large fluctuations which occur in the phase function (scattering diagram) for a single sphere. We have made preliminary computations to find the effect of changing the shape of the size distribution; the results for several different distributions indicate that the volume extinction (σ_{ext}), the single scattering albedo (ω), the asymmetry factor ($\langle\cos\theta\rangle$), and the shape of the phase function (oustide the region of the glory) depend mainly on

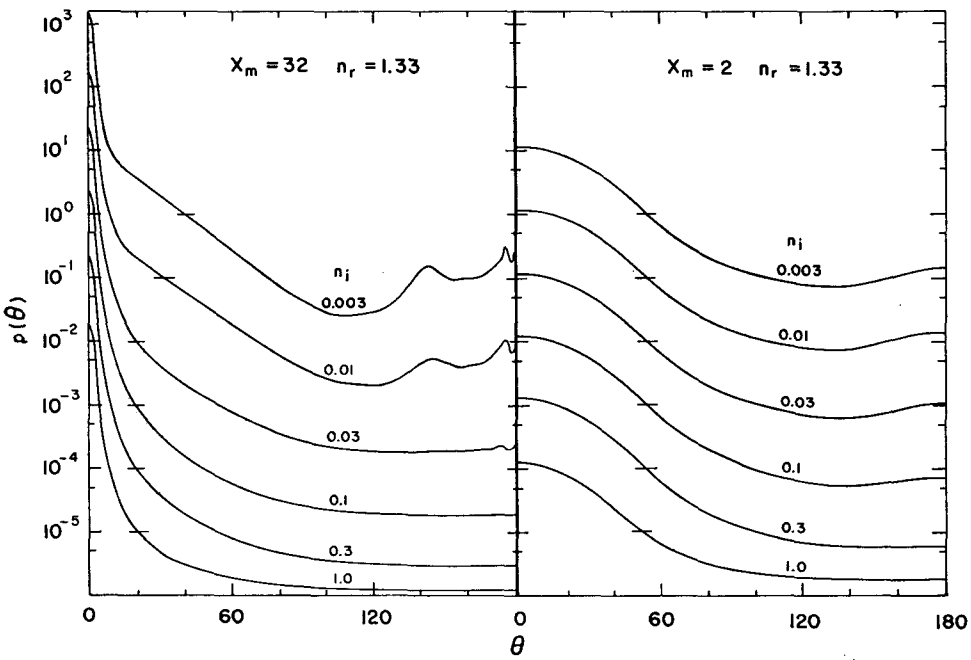

FIG. 2. Single-scattering phase functions for a size distribution of spherical particles showing the effect of absorption within the particles for large particles ($x_m = 32$) and particles of moderate size ($x_m = 2$).

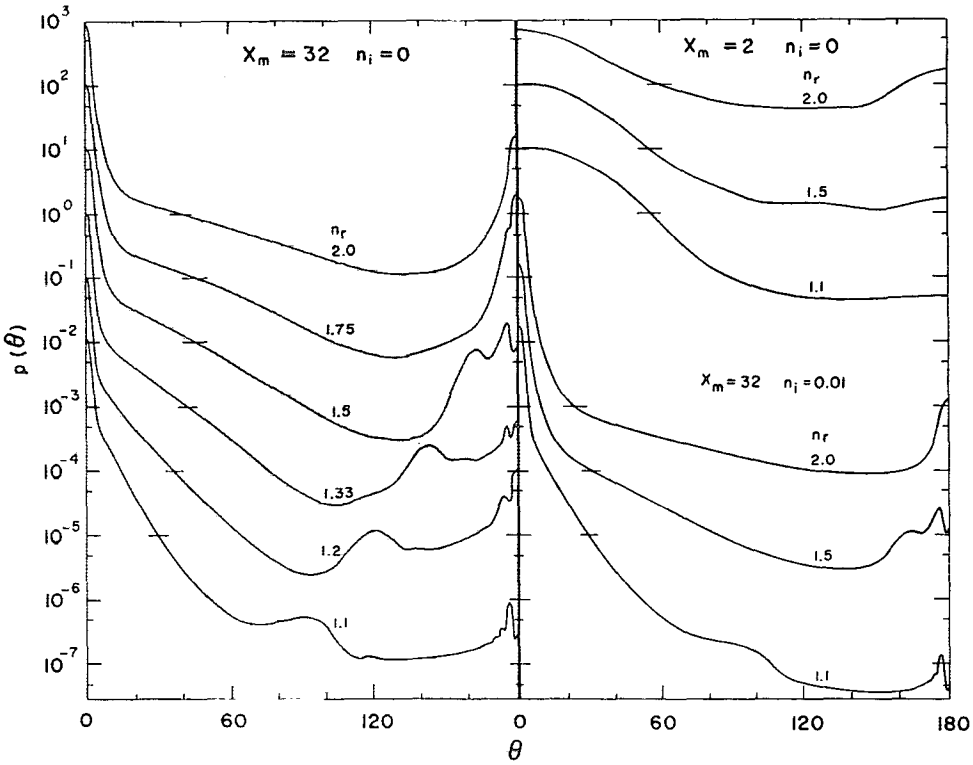

FIG. 3. Single-scattering phase functions for a size distribution of spherical particles showing the effect of changing the real part of the refractive index for large particles with no absorption (left), for particles of moderate size with no absorption (upper right), and for large particles with moderate absorption (lower right).

the mean particle radius for extinction; thus,

$$\bar{r} = \int_0^\infty \sigma_{\text{ext}}(r) n(r) r dr \Big/ \int_0^\infty \sigma_{\text{ext}}(r) n(r) dr, \qquad (2)$$

and not on the shape of the size distribution. This indicates that our computations in this paper with a single type of size distribution are meaningful, although in cases where a more exact knowledge of the size distribution is available, it should of course be used. For this paper (except in Section 3a) our computations were made with $r_m = 2$, 4, 8, 16 and 32 μ with the integrations over particle size extended to the radius $r_{\max} = 25\ \mu$ for the first four distributions and to $r_{\max} = 50\ \mu$ for the case $r_m = 32\ \mu$. The integration increments were chosen small enough to make the phase function smooth (see, e.g., Dave, 1969a, b). The values used for $r_{\max}$ were somewhat arbitrary but that is not essential since the purpose of the integration over particle sizes was to smooth out single particle effects; we usually found $\bar{r} \approx r_m$.

Except where otherwise indicated we employed the optical constants for water and ice tabulated by Irvine and Pollack (1968); the computations were made at each wavelength (~50) at which the authors tabulate the optical constants for the region of interest ($1.2 \geq \lambda \geq 3.6\ \mu$).

The intensity of light multiply scattered by the clouds was obtained by using the "double only" computing method. described by Hansen (1969a) which is a variation of van de Hulst's (1963) doubling method. If errors $\lesssim 1\%$ are tolerable, as is certainly the case for comparison to most observations, then the computing time may be greatly speeded up. Some of the more useful shortcuts which we have tested are described in the Appendix.

3. Results for single scattering

The single-scattering behavior of an ensemble of aerosols is a function of the complex index of refraction, $n_c = n_r - in_i$, and the distribution of particle sizes, expressed in units of the ratio x of the circumference of the particle to the wavelength, i.e., $x = 2\pi r/\lambda$. Assuming that the distribution of size is given by (1), we find that the parameter x_m, which equals $2\pi r_m/\lambda$, serves to define the dependence of the scattering behavior upon particle size. The results described below are of both general interest and of help in understanding the infrared properties of terrestrial clouds analyzed in later sections. In the calculations for Figs. 1–3 the integrations over the size parameter x were performed to an upper limit of $x_{\max} = 2x_m$, except when $x_m = 128$ for which $x_{\max}$ was set equal to 200.

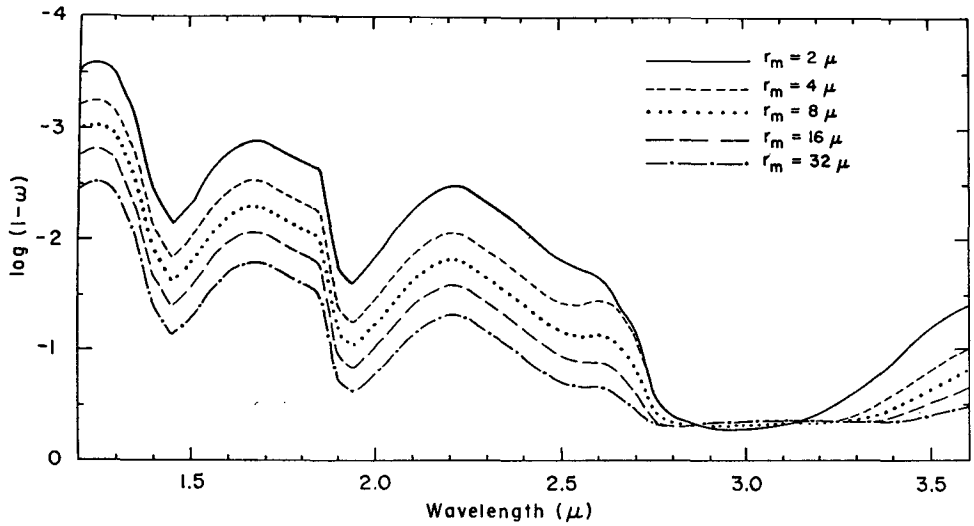

FIG. 4. Single-scattering albedo for a cloud of spherical water particles for five different particle size distributions.

a. General single-scattering results

Fig. 1 shows the dependence of the normalized phase function $p(\theta)$ (Deirmendjian, 1964, 1969) upon the particle size parameter x_m in the case of no absorption ($n_i=0$) with the real refractive index equal to 1.33, the value for liquid water in the visible. The variable θ is the angle of scatter.

The individual curves have been vertically displaced from one another. The short horizontal line intersecting a given phase curve denotes the position at which the phase function has a value of unity. For the largest values of x_m, the very precipitous decline in the value of p near 0° corresponds to the diffraction peak (Deirmendjian, 1964; Dave, 1969c); the strong maximum at a scattering angle of 142° is the main rainbow (caused by rays undergoing a single internal reflection) with its first supernumery bow (van de Hulst, 1957, p. 241) located at 147°; the second rainbow (two internal reflections) is located at 123° while its first supernumery bow lies at 114°; and finally, the glory corresponds to the overall increase and oscillatory behavior near 180°. As x_m decreases, all these features become less pronounced and broader; in addition, the rainbow shifts in location toward larger scattering angles and the slope of the phase function decreases until near $x_m=1/2$ it is very similar to the Rayleigh phase function.

The effect of introducing absorption within the particles is investigated in Fig. 2. For $x_m=32$, the glory and rainbow have been effectively suppressed when $n_i \gtrsim 0.03$. This effect can be understood using concepts from geometrical optics. A ray traversing a path equal to the particle radius will be diminished in strength by $\exp(-kr)=\exp(-2xn_i)$, where k is the linear absorp-

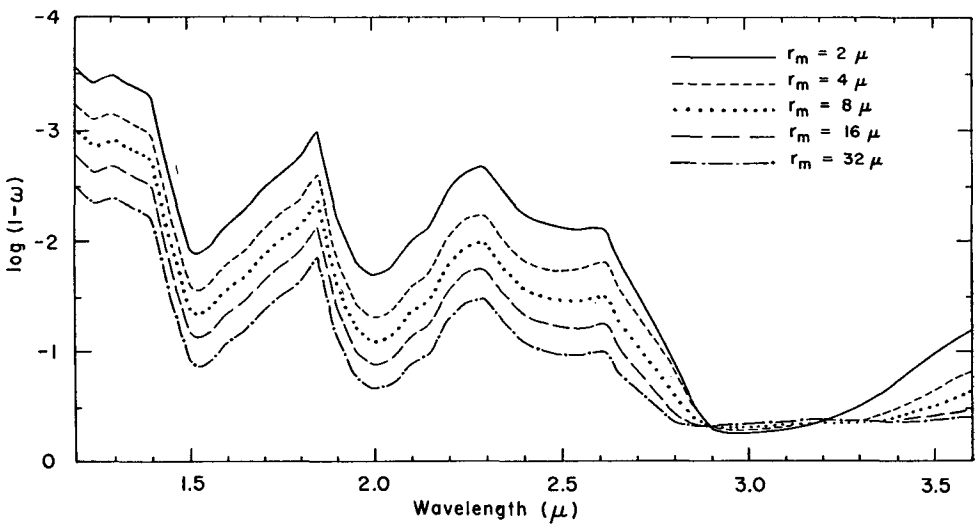

FIG. 5. Same as Fig. 4 except for spherical ice particles.

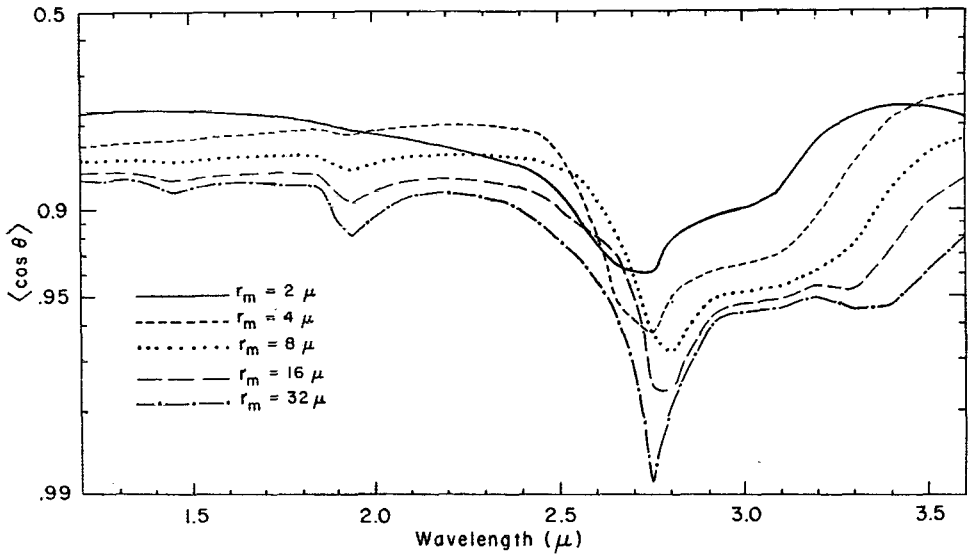

FIG. 6. Asymmetry factor of the phase function for a cloud of spherical water particles for five different particle size distributions.

tion coefficient. Setting n_i equal to 0.03 and x to 32, we see that the ray is diminished by almost a factor of 10 in intensity. Similarly, the diffraction component which is not affected by absorption extends to larger scattering angles as n_i increases.

For x_m again of 32, the value of the phase function in the backward hemisphere ($\theta > 90°$) begins to increase as n_i becomes $\gtrsim 0.1$. This may be attributed to an enhanced value of externally reflected light, as seen from the Fresnel equation. For the smaller particles ($x_m = 2$) the results are basically similar, although less pronounced.

Finally, we study the influence of the real part of the index of refraction in Fig. 3. For $x_m = 32$, increasing n_r causes the rainbow to shift to larger scattering angles, until it merges with the glory, resulting in a large increase in $p(180°)$. Aside from the diffraction peak, small-angle scattering becomes more dominant as the refractive index decreases, a result which shows up in the asymmetry factor $\langle \cos\theta \rangle$ described below. We will find this effect to be of significance in understanding certain spectral characteristics of water clouds. Similarly, at the lower values of n_r, refraction tends to dominate over diffraction at smaller angles of incidence and hence the break in the diffraction peak occurs at smaller values of θ. The right-hand half of the figure shows that similar effects occur for particles with absorption ($n_i = 0.01$) and for small particles ($x_m = 2$).

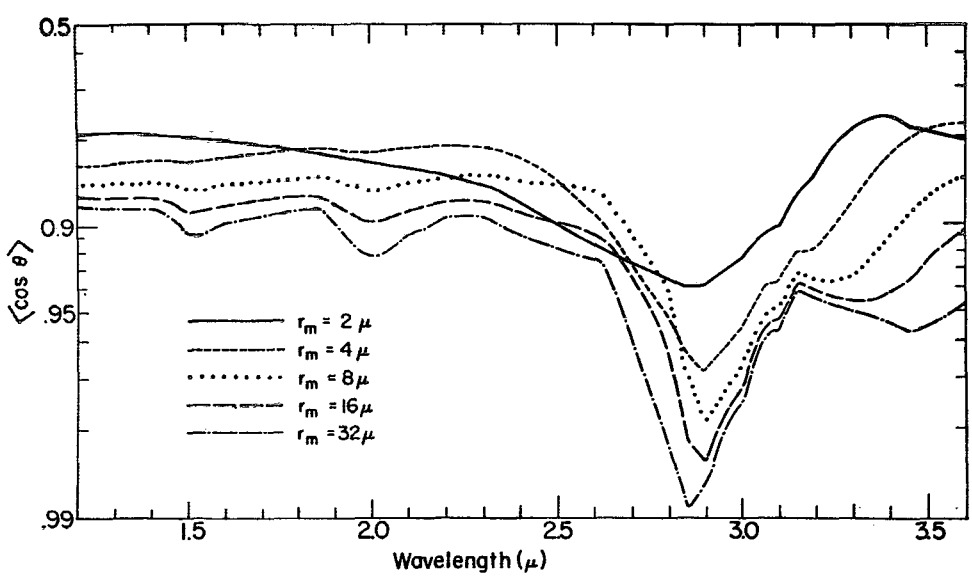

FIG. 7. Same as Fig. 6 for spherical ice particles.

b. Single scattering for water and ice

One important integral scattering parameter is the single-scattering albedo $\tilde{\omega}$, the ratio of the amount of light scattered to that which is scattered and absorbed. In Figs. 4 and 5 the spectral variation of $1-\tilde{\omega}$ is exhibited for liquid water and ice particles, respectively, for five values of the size parameter r_m.

As noted by Irvine and Pollack (1968), the maxima and minima of ice and water are displaced by about 0.1 μ in wavelength, a feature useful in distinguishing the phase of water clouds. Also, the single-scattering albedo generally declines monotonically with increasing particle size. It should be noted that in all cases $x_m > 3$. For sizes much smaller than this the particles will become completely absorbing and the above generalization is no longer true (van de Hulst, 1957). An interesting mild deviation from the general variation of $\tilde{\omega}$ with particle size occurs near a wavelength of 3 μ and may be due to the perturbing effect of the smallest particles having values of $x<1$. Near 3 μ the value of n_i is so large that the particles become completely opaque so that allowing for the diffraction peak $\tilde{\omega} \approx 1/2$.

The asymmetry factor $\langle\cos\theta\rangle$ is defined as the solid angle average of $\cos\theta$ weighted by the phase function. It describes the degree of forward scattering of the phase function. For isotropic scattering it has a value of zero while it approaches unity as small-angle scattering tends to dominate. Figs. 6 and 7 show the spectral behavior of $\langle\cos\theta\rangle$ for liquid water and ice particles, respectively. For the largest value of x_m there is a very pronounced increase in $\langle\cos\theta\rangle$ slightly shortward of 3 μ and a less obvious minimum somewhat longward of 3 μ. This behavior reflects the anamolous despersion changes in n_r near the very strong absorption feature centered near 3 μ, with changes in n_i also influencing $\langle\cos\theta\rangle$ near its minima. As shown in Fig. 3 and discussed earlier, the phase function becomes more forward scattering as n_r approaches unity.

From multiple-scattering computations reported below and elsewhere (Hansen, 1969a; Hansen and Cheyney, 1968) we find that for wavelengths $<2.5\,\mu$ and between 3.4 and 3.6 μ the reflectivity of thick clouds depends primarily on the single-scattering albedo; qualitatively, the curves of log $(1-\tilde{\omega})$ are very similar to the spectral variation of the cloud reflectivities. As the single-scattering albedo decreases, the less probable it is for a photon to survive a number of scattering events. Since the single-scattering albedo in these wavelength regions varies systematically with the characteristic particle size r_m (cf. Figs. 4 and 5) we can obtain particle size information from the near-infrared spectral behavior of clouds, as has been pointed out by Sagan and Pollack (1967), Hansen and Cheyney (1968), and Irvine and Pollack (1968).

On the other hand, in the spectral region between 2.5 and 3.4 μ the single scattering albedo has a constant value of about 1/2 and the spectral behavior of the cloud reflectivity depends primarily on $\langle\cos\theta\rangle$. There is an inverse qualitative similarity between the wavelength variation of $\langle\cos\theta\rangle$ and computed cloud reflectivities. As $\langle\cos\theta\rangle$ increases, less light incident on a cloud layer is reflected back out in the first few scattering events. If the single-scattering albedo is sufficiently less than one so that these scattering events are the major producers of reflected photons, the cloud reflectivity will decrease as $\langle\cos\theta\rangle$ increases. For example, the maximum in $\langle\cos\theta\rangle$ slightly shortward of 3 μ results in a minimum value for the cloud reflectivity at the same wavelength, as shown below. The spectral variation of $\langle\cos\theta\rangle$ is a reflection of the spectral behavior of the indices of refraction.

4. Reflectivity measurements of terrestrial clouds

Blau *et al.* [1966; see Blau and Espinola (1965) for a more detailed report] have obtained airborne infrared measurements of the reflectance properties of terrestrial clouds. These consist of both spectral and angular observations. Observations were performed from an aircraft above the cloud of interest and on a given day measurements were made either in the 1.2–2.5 μ region or the 2.4–3.6 μ wavelength domain. In addition, on some occasions angular scattering information was obtained by flying along a hexagonal path and performing spectral measurements of the cloud area situated at the center of the hexagon. In such measurements the angles of reflection and incidence remain constant, while the azimuth and angle of scatter vary. Below we describe these observations in greater detail and outline the transformation we applied to them so as to be be able to compare them with our multiple-scattering computations.

The spectral radiance (specific intensity) I_λ values reported by Blau *et al.* refer to averages of a number of spectra obtained close together in time. In addition, they also give values for the standard deviation of each average value. The standard deviation is not necessarily a reflection of the error of measurement, because it also includes short-term variations in the properties of the observed cloud. We subjected these measurements to two types of transformations. First we divided the observed specific intensity by the solar flux F_λ outside the atmosphere of the earth to obtain

$$R_\lambda = \frac{I_\lambda}{\mu_0 F_\lambda/\pi} = \frac{S}{4\mu\mu_0}, \tag{3}$$

where S, defined by Eq. (3), is the usual scattering function, $\theta_0 = \cos^{-1}\mu_0$, i.e., the angle of incidence, and $\theta = \cos^{-1}\mu$, the angle of reflection. If the clouds were a lambert surface, i.e., if they scattered isotropically, the normalized reflectivity R_λ would equal the spherical albedo of the clouds and would exhibit no angular variation.

TABLE 1. Water vapor amounts and cloud temperatures (after Blau *et al*).

Fig.	θ_0 (deg)	θ (deg)	Cloud	Cloud top altitude (10^3 ft)	P (atm)	W_{eff} (precipitable cm)	W_{ref} (precipitable cm)	T_{scat} (°K)	T_{cd} (°K)
				$\lambda = 1.2-2.5\,\mu$					
55	64	0	cirrus	38	0.5	0.26	0.0023	247	216
55	71	0	cirrus	38	0.5	0.20	0.0031	245	216
53	44	0	cumulus	28	1.0	0.68	0.014	260	233
51	52	0	thick cirrus over cumulus	25	0.5	0.10	0.061	239	238
				$\lambda = 2.4-3.6\,\mu$					
18	48	0	cumulus	50	0.2	0.0036	0.016		220
20	52	80	cirroform*	50	0.2	0.019	0.025		216

* Part of hurricane Gladys.

All the spectra show absorption features due to water vapor. In addition, some absortpion due to carbon dioxide at 2 μ is expected and there are strong CO_2 absorption features near 2.7 μ. Because gaseous absorption takes place not only above the clouds but through multiple reflection within the clouds, we did not exactly correct for this effect. One cannot practically correct for the multiple scattering within the clouds by assigning an effective single-scattering albedo to the gaseous absorption component, because the spectral resolution was much larger than the spectral domain over which the gaseous absorption is constant. We performed our water vapor absorption corrections by comparing the value of R_λ at two spectral positions, one position expected to have very little gaseous absorption and the other a large amount. Furthermore, the clouds were expected to have approximately the same intrinsic value for R_λ at the two wavelength positions. In the 1.2–2.5 μ region we compared R_λ values at 1.28 μ with either 1.35 μ or 1.38 μ, while for the 2.4–3.6 μ domain we considered values either at 2.50 or 2.55 μ with ones at either 2.60 or 2.61 μ. The ratio of the values of R_λ were equated to ratios of gaseous transmissivities calculated by Wyatt *et al.* (1962). The comparison was made at pressures and temperatures closest to the cloud top conditions, as inferred from the cloud top altitude, and in all cases at an effective resolution of 100 cm^{-1}. While this resolution is somewhat poorer than the resolution of the spectrometer, it was found to yield the most consistent results. In part, the need to employ 100 cm^{-1} resolution is a reflection of the breakdown of the theoretical statistical model at finer resolutions, as indicated by the appearance of high-frequency features whose amplitude is too large. From the comparison with Wyatt *et al.*'s tables we derived an effective water vapor abundance W and used this amount to estimate the effective gaseous transmission at other wavelengths. At wavelengths where there is more absorption by the cloud aerosols, there is less multiple scattering and in this sense the transmission correction is an overestimate. This circumstance pertains at most of the other wavelengths and the true cloud reflectivity, in general, should lie between the uncorrected and "corrected" values.

Absorption effects by CO_2 were much more localized in the spectrum. For the strong absorption band near 2.7 μ, we derived an effective amount of CO_2 and an average pressure by allowing for the path down to and up from the cloud top and estimating the effective path in the clouds from the water vapor absorption amount. The latter can be related to the atmospheric temperature where the absorption takes place, as discussed below, and to the path length with the help of the *U. S. Standard Atmosphere Supplements* (1966). For the much smaller corrections within the 2 μ band, we used the water vapor absorption amounts as a guide in a less rigorous fashion. Transmission corrections were then obtained from the tables of Stull *et al.* (1963).

Fortunately, since the angular measurements refer to the path lengths of nearly constant angle of incidence and reflection, they require no absorption correction to first order. However, because some absorption takes place through multiple scattering, the effective atmosphere transmission may have an azimuthal dependence. This effect is very difficult to correct for and no attempt was made to do so.

5. Discussion of gaseous absorption corrections

In Table 1 we summarize the water vapor amounts W_{eff} deduced from Blau *et al.*'s spectra. The first column gives the figure number of the spectra in their final report, and P is the pressure assumed in deriving W_{eff}. Also given are the cloud type and the cloud top altitude. Using the *U. S. Standard Atmosphere Supplements*, we have estimated the temperature T_{cd} at the cloud top from its altitude.

To assess the contribution of multiple scattering within the clouds to the observed water vapor absorption features, we have computed the equivalent amount of water vapor W_{ref} which the sunlight passes through above the clouds, on its path down to the cloud top and up to the airplane. In performing the calculation we

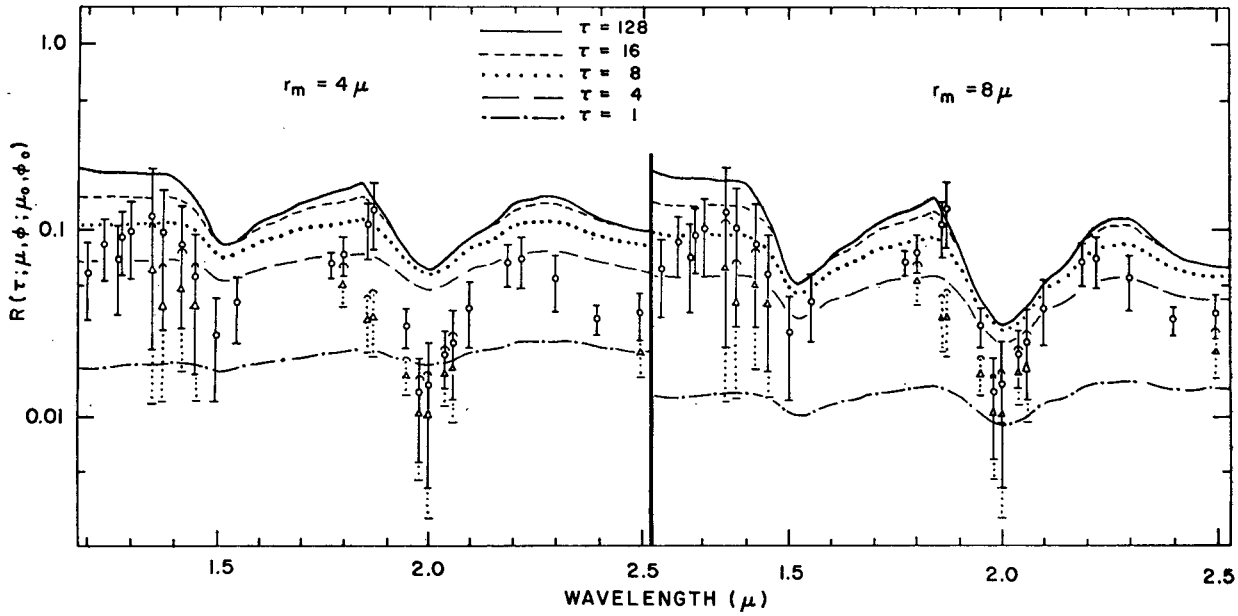

FIG. 8. Theoretical cloud reflectivities for $\theta=0$, $\theta_0=71°$ and $\phi-\phi_0=180°$ for five cloud optical thicknesses and two size distributions of spherical ice particles. The circles and solid bars represent observations by Blau *et al.* of cirrus clouds at 38,000 ft after correction for gas absorption; the uncorrected observations are indicated by triangles and dotted bars in the cases where they differ significantly from the "corrected" values.

have assumed the atmosphere to be saturated. In addition we have corrected for the difference in the value between the pressure used in obtaining W_{eff} and the actual cloud top pressure by assuming that pressure and gas amount are equally effective in causing absorption. For the first three spectra of the 1.2–2.5 μ region, W_{ref} is significantly smaller than W_{eff}. Hence, most of the absorption takes place in the clouds. A confirmation of this deduction is obtained by comparing the values of W_{eff} for the two sets of spectra from Blau *et al.*'s Fig. 55. The value of W_{eff} obtained for the larger angle of incidence is smaller than that for the smaller angle of incidence; this finding is opposite to the expectation for absorption taking place above the cloud, but in accord with predictions for multiple scattering within a cloud layer (Chamberlain, 1965). Such a phenomenon is also present for at least some of the gaseous absorption features of Venus (Chamberlain and Kuiper, 1956).

On the other hand, W_{ref} is larger or comparable to W_{eff} for the two spectra pertaining to the 2.4–3.6 μ region. This results in part from the cloud tops being located high within the stratosphere where the water vapor abundance is only a few per cent of the saturation abundance. For these spectra we can conclude that the fraction of the cloud significantly contributing to the scattering lies within the stratosphere and we are therefore surely viewing ice particles. The relatively small depth of penetration for these spectra is a result of the highly absorbing nature of ice aerosols at 2.5 and 2.6 μ, the wavelengths at which W_{eff} was obtained.

To derive an estimate of the depth of penetration for the other clouds, we have computed T_{scat}, the base temperature required within a saturated atmosphere so that light traveling on a straight line down to and up from this level at a 60° angle would experience the observed amount of absorption. Since the actual path length within the clouds is more tortuous, T_{scat} is probably a slight overestimate of the level of line formation. We see, for the first three spectra, that T_{scat} is substantially larger than T_{cd}, implying substantial penetration within the clouds. At the wavelengths used to derive W_{eff} for these spectra, the cloud aerosols are essentially transparent.

6. Analysis of the cloud spectra

Our theoretical spectra are functions of three parameters: the characteristic particle size r_m, the optical thickness τ of the clouds, and the phase of the cloud, i.e., whether the aerosols are liquid water or ice. We now attempt to estimate each of these parameters by comparing the theoretical and observed spectra.

In Figs. 8 and 9 Blau *et al.*'s observations of a cirrus cloud in the 1.2–2.5 μ wavelength region are compared with theoretical spectra for an ice cloud. The observations correspond to Blau *et al.*'s Fig. 55 for an angle of incidence of 71°. Circles and solid bars represent the average values and standard deviations of the reflectivity R [Eq. (3)] after correction for gas absorption, while the uncorrected observations are indicated by triangles and dotted bars in the cases where they differ significantly from the corrected values. As explained earlier, the absorption corrections may be overestimates in regions where the cloud aerosols strongly

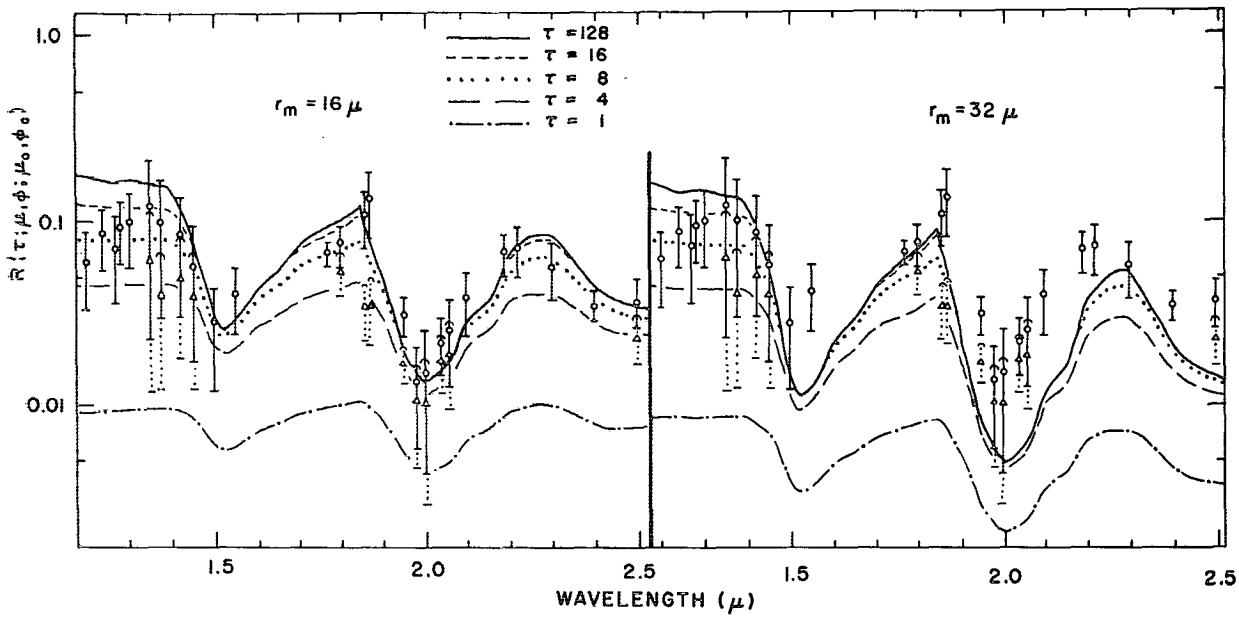

FIG. 9. Same as Fig. 8 for two additional particle size distributions.

absorb. In this case the true reflectivity will be somewhere between the corrected and uncorrected values. The theoretical curves in each portion of the diagrams correspond to various choices for the optical depth; the particle size parameter is varied by a factor of 2 between successive sections. Comparing the four sections of Figs. 8 and 9, we see that the observations permit the determination of a well-defined value of 16 μ for r_m.

In all of the figures the optical depth refers to $\lambda = 1.2\,\mu$; however, the wavelength dependence of τ is small since we always consider a distribution of particle sizes with $x_m > 1$. In determining τ, values of R between 1.2 and 1.4 μ are of particular use; the theoretical curves differ at these wavelengths by a maximum amount. For the cloud observations illustrated in Fig. 9 a value $\tau \sim 10$ appears to give the best fit. However, the optical depth is more difficult to estimate than the particle size, and this derived optical depth should probably only be regarded as a lower limit. Danielson *et al.* (1969) have argued, from observations and computations, that condensation nuclei limit the cloud reflectivity at wavelengths where ice and water do not effectively absorb $(1-\omega \lesssim 10^{-3})$.

As mentioned above, the absorption features of water and ice are displaced somewhat from one another. For example, peak absorptions and hence minimum values of R occur at 1.45 and 1.95 μ for water and at 1.52 and 2.00 μ for ice. As a result the theoretical water spectra do not fit the observed spectra in these regions. On the other hand, there is some indication that a local maximum in R occurs at 2.2 μ, a position expected for water clouds, rather than 2.3 μ, the place for ice clouds. A similar situation was found in some of the other spectra. This could be understood in terms of a mixed phase model with ice predominating near the top of the cloud, but the quality of the present data did not warrant calculations for such a model.

In a similar fashion we analyzed several other observed spectra. The results are summarized in Table 2. It is encouraging to see that the same cloud properties were found from observations of the same cloud viewed at two different solar illumination angles (Fig. 55). An interesting feature of Table 2 is the similar value for r_m found for the various ice cloud spectra. The deduced average particle radius of 16 μ, or diameter of 32 μ, is consistent with values typically obtained from direct sampling measurements of ice clouds.

In Fig. 10 we consider the degree to which multiple scattering occurs in the 2.5–3.5 μ spectral region, where the cloud aerosols are highly absorbing. The curves illustrated are for an optical depth of unity and a large enough optical depth ($\tau = 128$) to be considered

TABLE 2. Deduced properties of some observed terrestrial clouds.

Blau's Fig.	θ_0 (deg)	Cloud	Deduced properties Phase	$r_m(\mu)$	τ
		$\lambda = 1.2$–$2.5\,\mu$			
55	71	cirrus	ice	16	10
55	64	cirrus	ice	16	10
53	44	cumulus	water	8	4
51	52	thick cirrus over cumulus	ice	16	10
		$\lambda = 2.4$–$3.6\,\mu$			
18	48	cumulus	ice	16	>5
20	52	cirroform	ice	16	>5

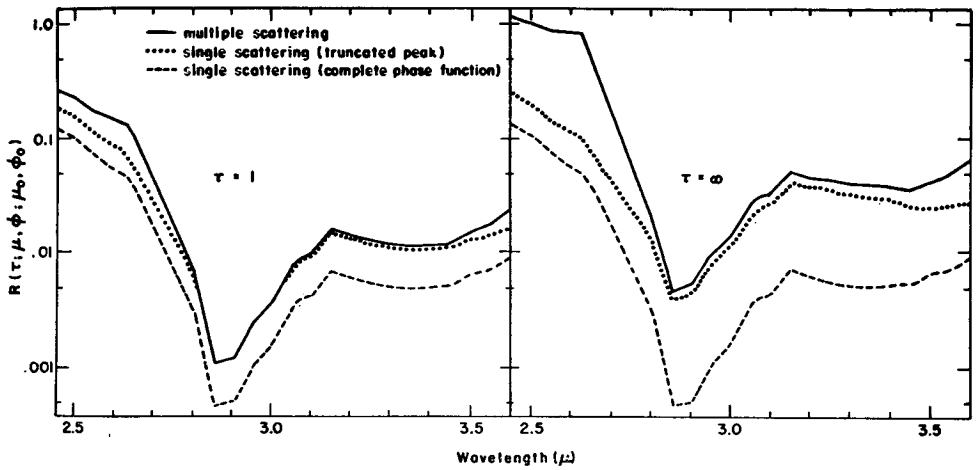

FIG. 10. Theoretical cloud reflectivities for $\theta=0°$, $\theta_0=48°$ and $\phi-\phi_0=180°$, for two cloud optical thicknesses for the size distribution of spherical ice particles having the characteristic particle size $r_m=16\,\mu$.

equivalent to an infinite value; we obtained almost identical results for all optical depths >10. The dashed curve represents photons scattered only once, the dotted curve photons scattered n times ($n\geq 1$) with the first $n-1$ scattering events occuring within the diffraction peak (Hansen, 1969b), while the solid curve represents all the photons reflected from the cloud. We see that even if the dotted curve is considered as representing single scattering, single-scattering computations are inadequate to describe the reflectivity in this highly opaque part of the spectrum.

In Fig. 11 we compare computed cloud spectra for $\tau\geq 10$ with data given in Blau *et al.*'s Figs. 18 and 20. The theoretical curves correspond to various choices of r_m. The data points between 2.5 and 2.6 μ indicate a particle size of about 16 μ in both cases. Near 3 μ the observations and calculations are not in good agreement; this disagreement is discussed in detail in Section 8.

Finally, we note that sample calculations of blackbody thermal emission from the clouds showed this contribution to be very small compared to reflected sunlight, even at the longest wavelengths of observation.

7. Analysis of the clouds' angular scattering

In this section we attempt to assess the information content of the clouds' angular scattering properties. As

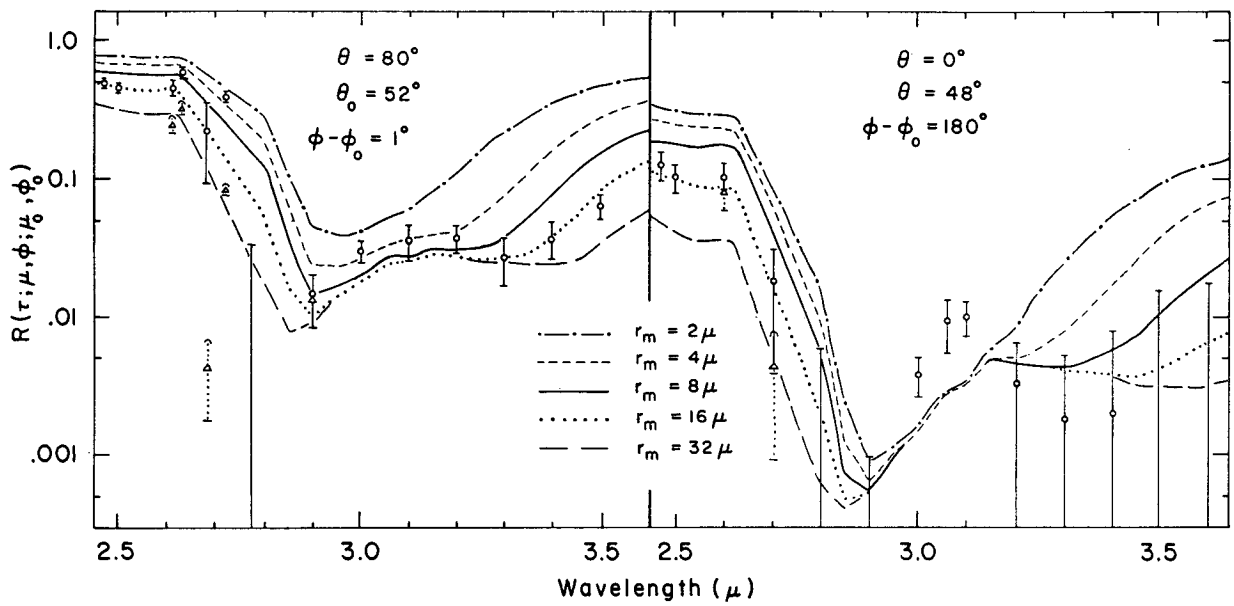

FIG. 11. Theoretical cloud reflectivities for $\tau\geq 10$ for five size distributions of spherical ice particles. The circles represent observations by Blau *et al.* of "cumulus" clouds at 50,000 ft after correction for gas absorption; the uncorrected observations are indicated by triangles.

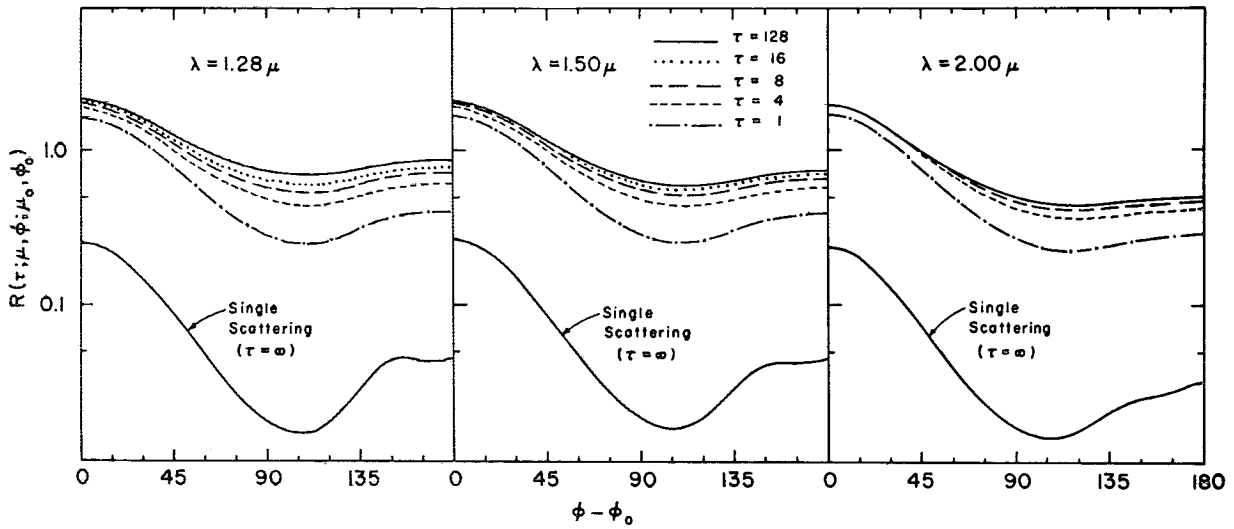

FIG. 12. Theoretical cloud reflectivities as a function of azimuth angle for $\theta=80°$ and $\theta_0=60°$ for a size distribution of spherical water particles with $r_m=2$.

mentioned earlier, observations were made at nearly constant angles of incidence and reflection but with varying azimuth and hence scattering angles. In Figs. 12 and 13 we contrast the theoretical single-scattering behavior of water clouds with the complete multiple-scattering behavior. The computations were made for angles of incidence and reflection of 60° and 80°, respectively. In Fig. 12 the reflectivity has been calculated for a distribution of water particles having a mean size r_m of 2 μ, while Fig. 13 pertains to a value of 16 μ for r_m. For the larger size particles, we defined single scattering to include photons scattered $(n-1)$ times in the diffraction peak $(n\geq 1)$ before suffering a final scattering back out of the cloud. Since the 2 μ particles do not have a striking diffraction peak, we defined single scattering for them in the conventional manner.

We see that the effect of multiple scattering is to wash out features such as the rainbow and to greatly diminish the angular variation of R. Even for an optical depth of unity the actual scattering behavior is markedly different from that of single scattering. At an optical depth of 16 the scattering behavior is quite close to that for an infinite optical depth. On the basis of their high albedo in the visible we know most clouds have an optical depth ≥ 16. In this event a knowledge of the exact value of the optical depth is not too important for being able to predict the reflectivity properties.

In Fig. 14 we compare theoretical calculations with the angular dependence exhibited by a cumulus cloud whose top was at 4000 ft. This cloud was part of hurricane Gladys. For each data point the angle of reflection was 80° but the angle of incidence varied between 56°

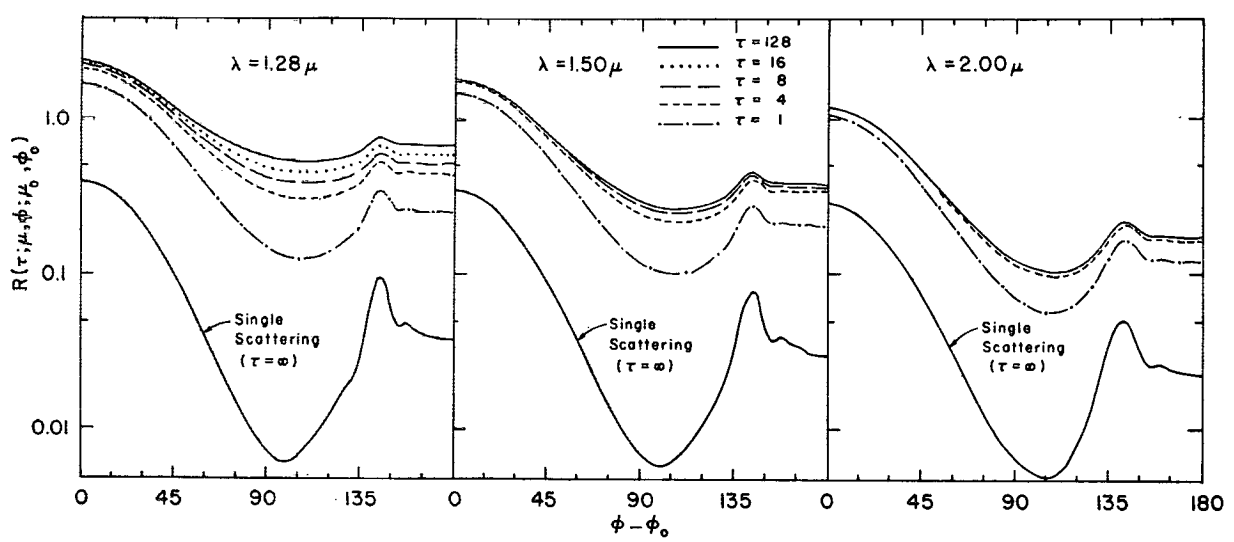

FIG. 13. Same as Fig. 12 for a size distribution with $r_m=16$.

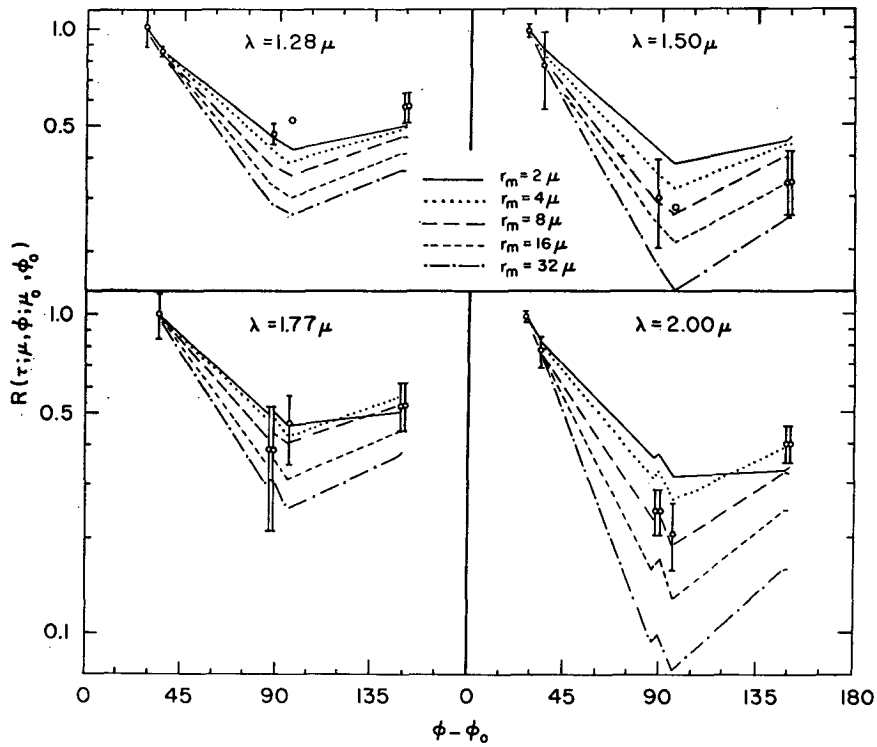

FIG. 14. Theoretical and observed cloud reflectivities for $\theta=80°$ and $56\leq\theta_0\leq64$ normalized to unity at the smallest observed value of $\phi-\phi_0$. The theoretical calculations are for water particles at values of θ, θ_0 and $\phi-\phi_0$, correct for each observed point and connected by straight lines. The computations were made for $\tau=32$, but are approximately valid for $\tau\geq10$. The observations by Blau *et al.* were made on cumulus clouds at 4000 ft above hurricane Gladys.

and 64°. The theoretical computations were performed for spherical water particles at the angles appropriate for each observation, and the theoretical points were joined together by straight lines. As mentioned above, no correction for gas absorption was made.

All the theoretical spectra are normalized to fit the data point at the lowest value of $(\phi-\phi_0)$. A particle size of 8 μ appears to yield the best fit to the measurements, a result compatible with typical direct sampling measurements of cumulus clouds. Unfortunately, the ab-

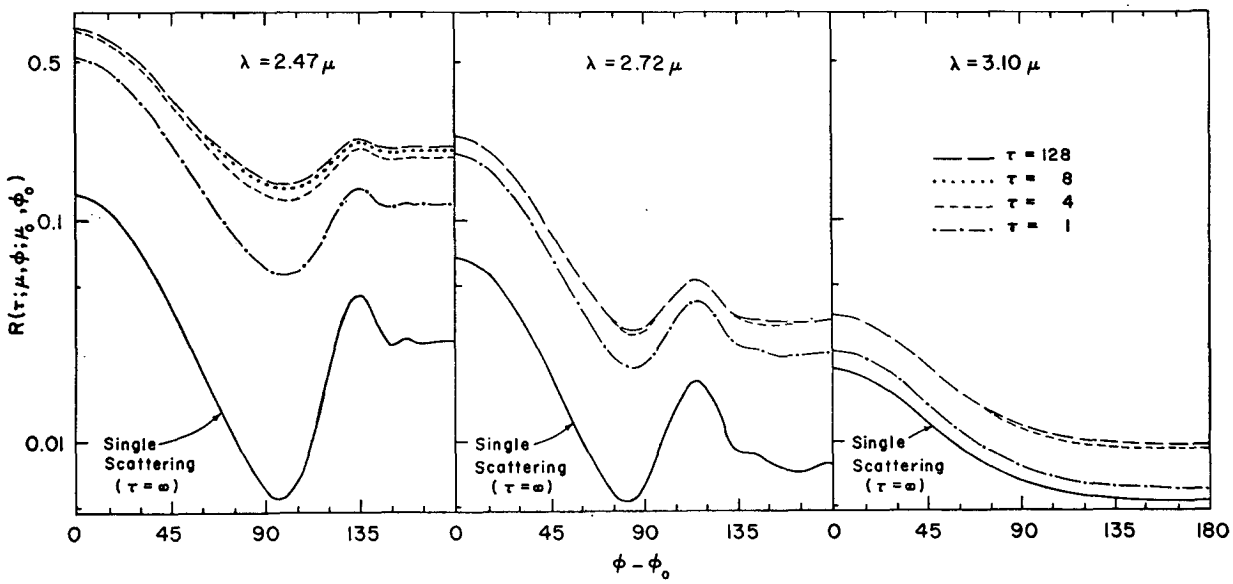

FIG. 15. Theoretical cloud reflectivities as a function of azimuth angle for $\theta=80°$ and $\theta_0=50°$ for a size distribution of spherical ice particles having $r_m=16\,\mu$.

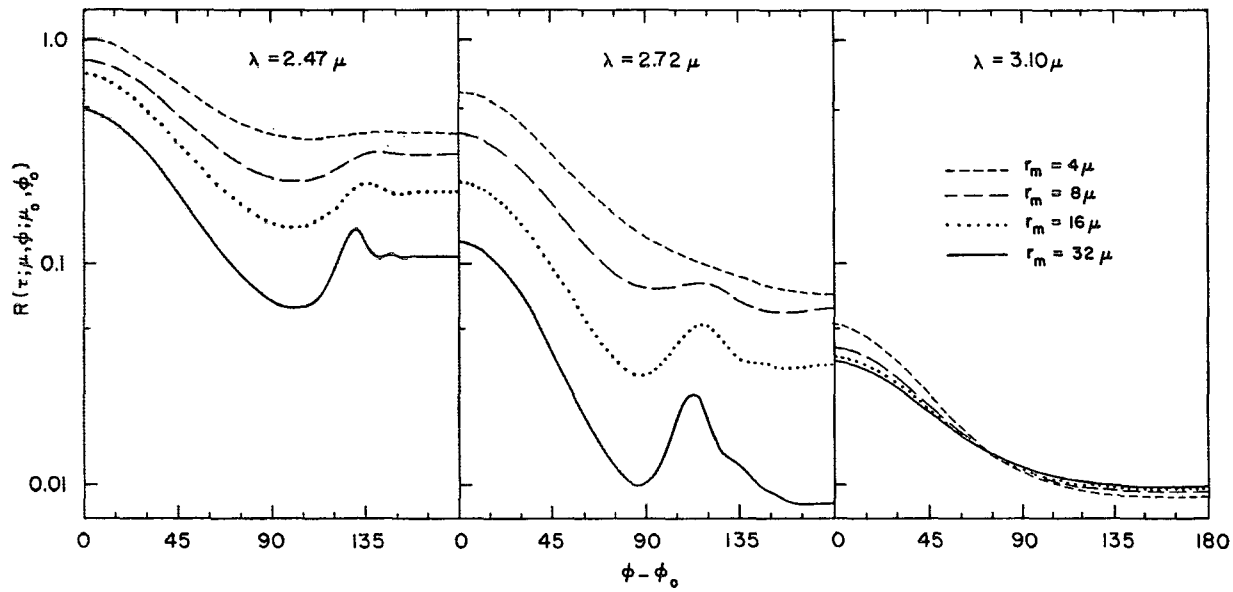

FIG. 16. Same as Fig. 15 but for four particle size distributions and for only one cloud optical thickness ($\tau=32$).

sorption corrections were so large we were unable to meaningfully analyze the spectra to confirm this deduction.

Angular computations in the 2.4–3.6 μ region are shown in Figs. 15 and 16. The calculations were made for spherical ice particles with the realization that this may lead to a very poor approximation to the true angular scattering behavior of ice clouds. In Fig. 15 a mean particle radius r_m of 16 μ was used and the optical depth varied. In Fig. 16 the particle size is varied, while the optical depth was set equal to 32. In all cases the angles of incidence and reflection are 50° and 80°, respectively. We see that for cases of intermediate aerosol absorption, e.g., $r_m=16\ \mu$ and $\lambda=2.72\ \mu$, the exact solutions most clearly preserve such features as the rainbow peak and exhibit the strongest dependence upon particle size. When the aerosol absorption is relatively small, many scattering events occur leading to a smooth, featureless angular behavior. When the aerosol absorption is very large the rainbow is not present even for single scattering.

In Fig. 17 we compare theoretical and observed cloud reflectivities for an angle of reflection of 80° and an angle of incidence between 44° and 56°. The observations pertain to cirroform clouds whose tops were at 43,000 ft. They were part of hurricane Gladys. The theoretical curves have the same meaning as those in Fig. 14, except that Fig. 17 is for spherical ice particles. A particle radius of 16 μ, a value found typical for cirrus clouds from the spectral analysis, gives no worse a fit to

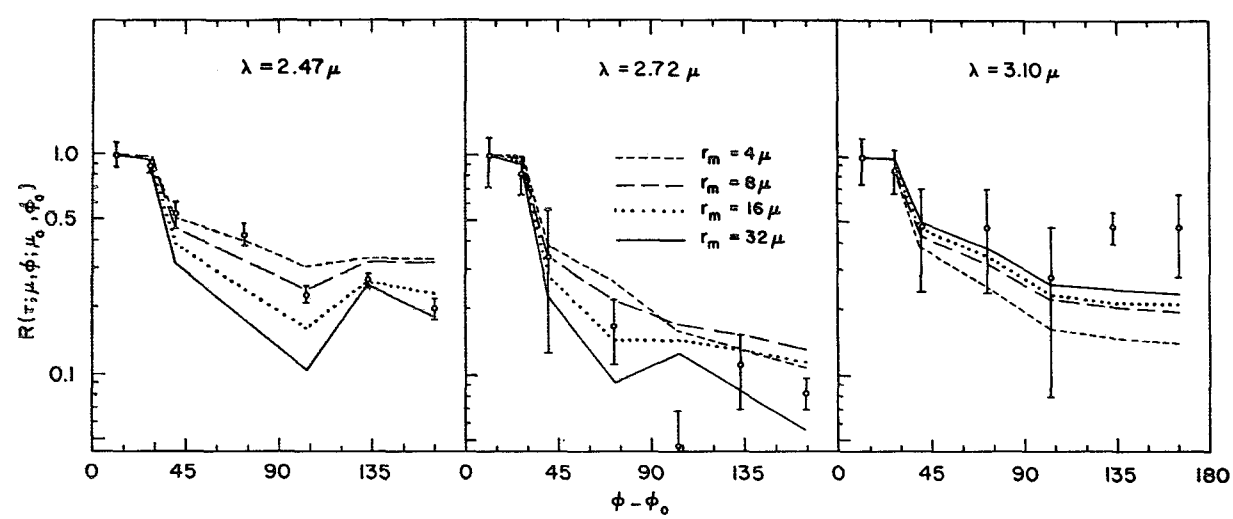

FIG. 17. Theoretical and observed cloud reflectivities for $\theta=80°$ and $44°\leq\theta_0\leq56°$, normalized to unity at the smallest observed value of $\phi-\phi_0$.

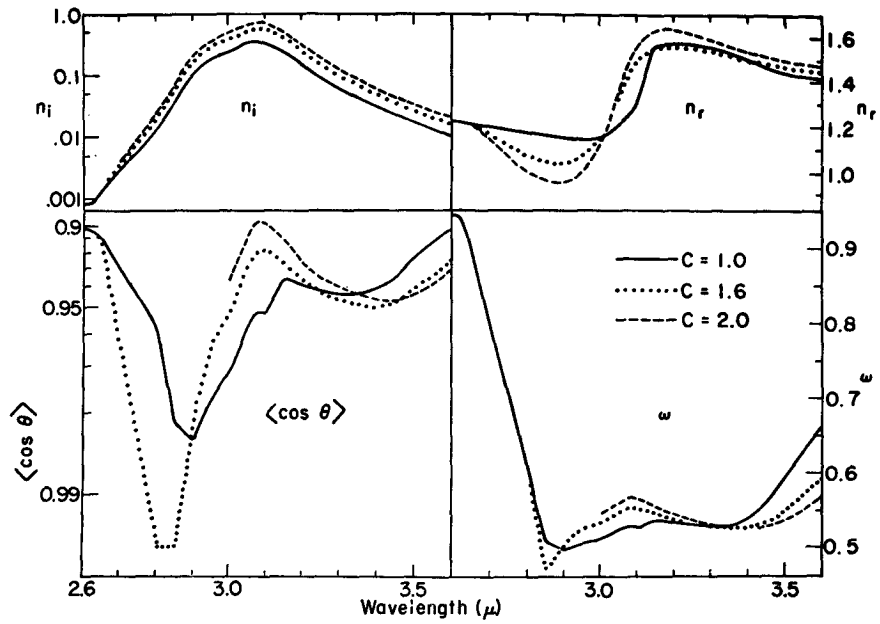

FIG. 18. The optical constants for ice (upper part) with the solid curve representing the data of Irvine and Pollack (1968); the other two curves were obtained by multiplying Irvine and Pollack's $n_r n_i$ by the factor c in the interval $2.8 \leq \lambda \leq 3.6$. The lower part of the figure shows the single scattering parameters $\langle\cos\theta\rangle$ and ω for the three sets of optical constants.

the data than other sizes. The calculations at all three wavelengths were made with the optical constants given by Irvine and Pollack; however, if we accept the modification in the optical constants which is indicated by the results in Section 8, then the theoretical calculations at $\lambda = 3.10\ \mu$ would be changed and brought into better agreement with the observations. At $3.10\ \mu$ the primary effect of the new optical constants is to increase the Fresnel reflection in the backward direction; this would increase the theoretical reflectivity at the two rightmost data points in Fig. 17.

8. Optical constants of ice near $\lambda = 3\ \mu$

In this section we reconsider the ice cloud spectra near $\lambda = 3\ \mu$ where the calculations and observations are not in good agreement, and we suggest one possible explanation for the discrepancy.

A minimum in the observed spectra (Fig. 11) occurs at about $2.9\ \mu$ in wavelength and a maximum around $3.1\ \mu$. These features are particularly prominent in the right-hand graph. This may at first appear surprising since ice has its maximum absorption at $3.1\ \mu$ (Irvine and Pollack, 1968). Blau and Espinola (1968) first pointed out the minima in the spectra and correctly attributed it to the anomalous dispersion of n_r, which is discussed above. A local maxima in the reflectivity is expected near $3.1\ \mu$ for similar reasons. Our computed spectra qualitatively show these effects, but particularly for the right-hand graph (Fig. 11) they fail to quantitatively match the observations. Blau and Espinola encountered a similar difficulty in explaining the minimum and suggested that Irvine and Pollack's value of n_r be revised near this wavelength position.

We have also considered the possibility of revising Irvine and Pollack's optical constants for ice in the vicinity of the strong $3.1\ \mu$ feature. We have attempted to do this in a consistent fashion by relating changes in the real part n_r, of the index of refraction, to changes in the imaginary part n_i. Spitzer and Kleinman (1961) have given relationships between n_r and n_i under the assumption that individual absorption bands may be considered as classical oscillators and have obtained a very good fit to reflection measurements of strong infrared bands of quartz. Assuming that the $3.1\ \mu$ band is a dominant feature at nearby wavelengths and neglecting small differences between the value of the frequency at the desired positions and the central frequency of the band, we have simplified Spitzer and Kleinman's formulas to the following general form:

$$n_r n_i = \frac{p\Gamma^2}{(\Delta\lambda)^2 + \Gamma^2}, \tag{4}$$

$$n_r^2 - n_i^2 = A + \frac{2p\Gamma\Delta\lambda}{(\Delta\lambda)^2 + \Gamma^2}, \tag{5}$$

where p is the maximum value of the product of $n_r n_i$, Γ one-half the value of the width between half maximum points of $n_r n_i$, $\Delta\lambda$ the difference in wavelength between the value of interest and the position of the maximum, and A a constant. These formulae give a good fit to the water and ice data of Irvine and Pollack near the

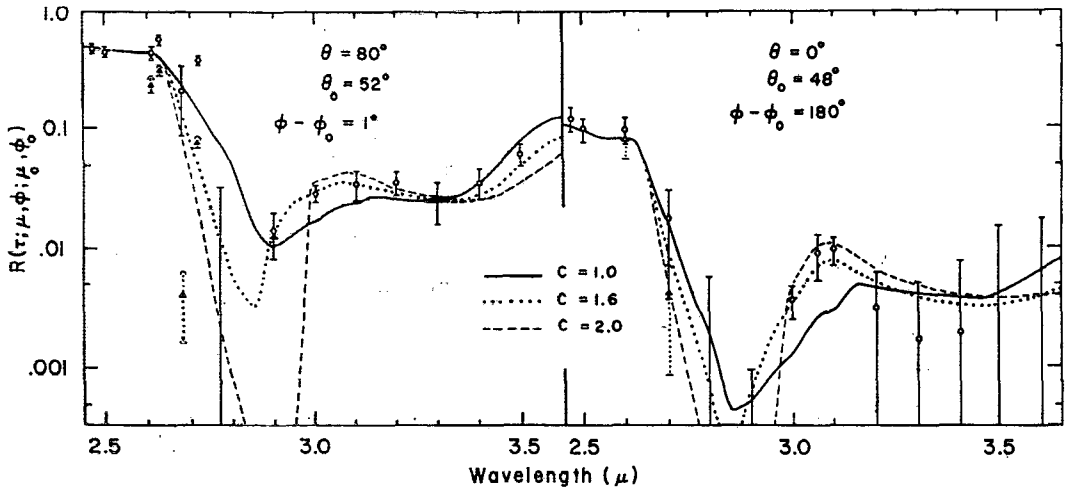

FIG. 19. Same as Fig. 11 with the theoretical curves for the size distribution having $r_m = 16\,\mu$; the three curves correspond to the three choices of c shown in Fig. 18.

3 μ absorption feature. For the ice constants given by these authors $p \approx 0.42$ and $\Gamma \approx 0.15\,\mu$. The constant A is readily found by applying the second formula to wavelengths significantly shortward of 3 μ; we find A is 1.66.

In modifying the indices of refraction given by Irvine and Pollack we assumed that Γ was unchanged and varied the only remaining free parameter p by various scale factors c. We have modified the published data between 2.8 μ and 3.6 μ because this is the region dominated by the 3.1 μ band. In addition, the published indices shortward of 2.8 μ were based on a different set of measurements than those used at 2.8 μ and longward. These first set were checked against other measurements and found to be in good agreement. The results of two trial modifications are given in Fig. 18 along with the original values. In addition, the effects of the modified indices on the single scattering albedo $\tilde{\omega}$ and the angular asymmetry parameter $\langle\cos\theta\rangle$ are shown. Since at short wavelengths the value $c=2$ led to values of $n_r < 1$, this portion of the curve has not been drawn.

Since the optical parameters have not been changed shortward of 2.8 μ, the deduced characteristic particle sizes and the lower limit on the optical depth will still hold. We were able to deduce these from the data points between 2.47 μ and 2.65 μ. Fig. 19 shows theoretical spectra for Blau's Figs. 18 and 20 based on values of $c=1$ (the old optical constants), 1.6 and 2. We see that a value of c of ~ 1.6 leads to a good fit of the spectra for both Figs. 18 and 20.

Some justification for our method of varying the constants is provided by the following: For wavelengths $< 2.8\,\mu$ the optical constants of Irvine and Pollack were based on several sources of data which agreed with one another. However, for $\lambda \geq 2.8\,\mu$ Irvine and Pollack had only one source for the ice absorption coefficients and this source gave water absorption coefficients for $\lambda \approx 3\,\mu$ which were $\sim 60\%$ less than the values obtained by several other experimenters. Thus, the proposed revision of the indices of refraction seems quite reasonable.

9. Summary

This study indicates that characteristic broad band absorption features in light scattered by clouds can be used to help identify the scattering material and to determine the particle size and cloud optical depth. The results are consistent with the assumption that it is adequate to employ the spherical particle approximation in calculating the *spectral* reflectivity. As far as the angular behavior is concerned, not enough accurate observations are available for an adequate analysis of the theory. More extensive measurements on atmospheric clouds are desirable, as well as carefully controlled laboratory observations along the lines of the recent measurements by Zander (1968) and Plummer (1969).

Acknowledgments We are very indebted to Henry Blau and Ronald Espinola for several useful discussions and for sending us some of their original data. This research was supported in part at Cornell University by by NASA Grant NGR 33-010-082 and NSF Grant GA-1086. During the course of this work J. Hansen was supported consecutively by a NAS-NRC Research Associateship supported by NASA at the Institute for Space Studies, a National Science Foundation Fellowship at the Sterrewacht, Leiden, Netherlands, and by NASA Grant 33-008-012 through Columbia University.

APPENDIX

Multiple Scattering Computations

The following shortcuts in the numerical work have been tested and found useful for the multiple scattering computations:

a. For large particles ($x = 2\pi a/\lambda \gtrsim 25$) there is a sharp diffraction peak in the phase function which necessitates a large number of terms in the cosine expansion of the

scattering function and a large number of points in the integrations over $\mu=\cos\theta$. However, in the case of conservative scattering we have shown elsewhere (Hansen, 1969b) that the photons scattered into the forward spike may be approximated as being unscattered by truncating the forward peak from the phase function and reducing the interaction optical thickness τ such that

$$\tau'=(1-F)\tau, \tag{A1}$$

where τ' is the optical thickness to be used with the truncated phase function, F the fraction of photons scattered into the forward peak, i.e.,

$$F=\int_{4\pi}(p-p')\frac{d\omega}{4\pi}, \tag{A2}$$

and p and p' are the untruncated and truncated phase functions, respectively. For conservative scattering this approximation introduces large errors in the reflected intensities only for small total scattering angles ($\theta\approx 0°$); it introduces errors of a few per cent if the total scattering angle corresponds to a sharp feature in the phase function (such as the glory), and it also introduces errors of a few per cent if the incident or emergent angle is near grazing (θ, $\theta_0\approx 90°$); elsewhere the error is $\lesssim 1\%$.

In the case of nonconservative scattering the single scattering albedo ω must be scaled such that

$$\omega'=1\Big/\left\{1+\left[\frac{1-\omega}{\omega(1-F)}\right]\right\}, \tag{A3}$$

because the assumption that photons in the forward peak should be treated as unscattered implies that the absorption cross section is unchanged and the scattering cross section reduced by the factor $1-F$. Several tests of this approximation were made and it was found to become increasingly accurate as ω decreased. Even in the wavelength region $\sim 3\,\mu$ where often $\sim 80\%$ of the single scattered photons were cut off with the truncating of the diffraction peak, the error introduced was $\lesssim 1\%$ except for scattering angles $\sim 0°$.

b. In the expansion of the scattering function in cosines, we write

$$S(\tau;\mu,\phi;\mu_0,\phi_0)=\sum_{m=0}^{\infty}S^m(\tau;\mu,\mu_0)\cos m(\phi-\phi_0), \tag{A4}$$

where μ_0 and μ denote the cosine of the angles of incidence and reflection, respectively, and ϕ_0 and ϕ the corresponding azimuth angles. The number of terms, M, needed to obtain an accuracy within 1% for all μ and μ_0 with a strongly anisotropic phase function is typically ~ 100. However, the range of μ and μ_0 for which the numerical value of $S^m(\mu,\mu_0)$ is not negligible decreases as m increases until for $m\approx M$ only $S(\tau;\mu\sim 0,\mu_0\sim 0)$ is significant. If $S(\tau;\mu,\phi;\mu_0,\phi_0)$ is to be calculated at N values of μ on the interval (0,1) and N values of μ_0, then $S^0(\tau;\mu,\mu_0)$ must be computed at N^2 points and in the integrations over μ which include $S^0(\tau;\mu,\mu_0)$ as a factor, N points are employed; however, the number of points required decreases steadily as m increases until for $S^M(\tau;\mu,\mu_0)$ calculations are only needed for one point and only one point is needed in the integrations. For a given accuracy specification it is easy by numerical testing to find the number of points at which $S^m(\tau;\mu,\mu_0)$ must be calculated and included in the integrations. A factor of 2–3 in computer time may be saved with an introduction of errors ~ 1–2%.

c. The strongest azimuthal dependence arises from single-scattered photons but an analytic expression exists for the intensity due to these photons (Hansen, 1969a); hence, considerable computing time may be saved by writing

$$S(\tau;\mu,\phi;\mu_0,\phi_0)=S_{ss}(\tau;\mu,\phi;\mu_0,\phi_0)$$
$$+\sum_{m=0}^{\infty}\left[S^m(\tau;\mu,\mu_0)-S_{ss}{}^m(\tau;\mu,\phi_0)\right]\cos m(\phi-\phi_0), \tag{A5}$$

where the subscript ss labels the contributions of single scattering to the S function. Typically, the number of terms needed in (A5) is $\sim 50\%$ of the number required with (A4) to achieve the same accuracy.

d. Several additional ways to save computer time, which we found by numerical experimentation, can be shown to have a firm theoretical basis from work of van de Hulst (forthcoming book) who shows that each term in the $\cos m(\phi-\phi_0)$ expansion may be thought of as having an effective albedo for single scattering and this albedo decreases steadily as m increases. Some consequences are: 1) the doubling process for terms with $m\geq 1$ may be initiated at an optical thickness $\tau_0\sim 2^{-15}$ rather than 2^{-25}; 2) for $m\geq 1$ the asymptotic value of the scattering function is obtained already at $\tau\sim 8$; and 3) for $m\gtrsim M/4$ the sum of the infinite series occurring in the doubling equations may be replaced by the value of the first term. These simplifications may easily reduce the computing time by a factor of ~ 3.

If all four of the above methods for reducing the computer time are employed, the total time saving is not the product of the factors which each gives alone because there is considerable overlap. In the computations for this paper (performed on an IBM 360/95) we always employed *d*, and for the particle size distributions with $r_m=16\,\mu$ and $32\,\mu$ we used *a*. All of the above methods may be worthwhile for slower computers and especially for problems such as line formation and the multiple scattering of polarized light.

Note added in revision. Dave and Gazdag (1970) have independently shown that the number of terms required in the Fourier expansion depends strongly on μ and μ_0 (shortcut *b* above) and they have presented graphical

illustrations of this. They also make use of the fact that the effective albedo decreases toward higher terms in the Fourier expansion (shortcut *d*).

REFERENCES

Blau, H. H., and R. P. Espinola, 1965: Infrared spectra properties of high-altitude clouds. Arthur D. Little, Inc., Rept., Cambridge, Mass, 117 pp.

—— and - - -, 1968: Spectral property of clouds from 2.5 to 3.5 microns. *Appl. Opt.*, **7**, 1897.

— , and E. C. Reifenstein, 1966: Near infrared scattering by sunlit terrestrial clouds. *Appl. Opt.*, **5**, 555–564.

Chamberlain, J. W., 1965: The atmosphere of Venus near her cloud tops. *Astrophys. J.*, **141**, 1184–1205.

——, and G. P. Kupier, 1956: Rotational temperature and phase variation of the carbon dioxide bands of Venus. *Astrophys. J.*, **124**, 399–405.

Danielson, R. E., D. R. Moore and H. C. van de Hulst, 1969: The transfer of visible radiation through clouds. *J. Atmos. Sci.*, **26**, 1078–1087.

Dave, J. V., 1969a: Effect of coarseness of the integration increment on the calculation of the radiation scattered by polydispersed aerosols. *Appl. Opt.*, **8**, 1161–1167.

——, 1969b: Effect of varying integration increment on the computed polarization characteristics of the radiation scattered by polydispersed aerosols. *Appl. Opt.*, **8**, 2153–2154.

——, 1969c: Scattering of visible light by large water spheres. *Appl. Opt.* **8**, 155–164.

——, and J. Gazdag, 1970: A modified Fourier transform method for multiple scattering calculations in a plane-parallel Mie atmosphere. *Appl. Opt.* (in press).

Deirmendjian, D., 1964: Scattering and polarization properties of water clouds and hazes in the visible and infrared. *Appl. Opt.*, **3**, 187–196.

——, 1969: *Electromagnetic Scattering on Spherical Polydispersions*. New York, Elsevier, 290 pp.

——, and R. J. Clasen, 1962: Light scattering on partially absorbing homogeneous spheres of finite size. Rept. R-393-PR, The RAND Corporation, Santa Monica, Calif., 44 pp.

Hansen, J. E., 1969a: Radiative transfer by doubling very thin layers. *Astrophys. J.*, **155**, 565–573.

——, 1969b: Exact and approximate solutions for multiple scattering by cloudy and hazy planetary atmospheres. *J. Atmos. Sci.*, **26**, 478–487.

——, and H. Cheyney, 1968: Near infrared reflectivity of Venus and ice clouds. *J. Atmos. Sci.*, **25**, 629–633.

——, and ——, 1969: Theoretical spectral scattering of ice clouds in the near infrared. *J. Geophys. Res.*, **74**, 3337–3346.

Irvine, W. M., and J. B. Pollack, 1968: Infrared optical properties of water and ice spheres. *Icarus*, **8**, 324–360.

Kattawar, G. W., and G. N. Plass, 1967: Electromagnetic scattering from absorbing spheres. *Appl. Opt.*, **6**, 1377–1382.

Plummer, W. T., 1969: Near-infrared reflection spectra of artificial cumulus clouds. *Appl. Opt.*, **8**, 2079–2081.

Pollack, J. B., and C. Sagan, 1968: The case for ice clouds on Venus. *J. Geophys. Res.*, **73**, 5843–5949.

Sagan, C., and J. B. Pollack, 1967: Anisotropic nonconservative scattering and the clouds of Venus. *J. Geophys. Res.*, **72**, 469–477.

Spitzer, W. G., and D. A. Kleinman, 1961: Infrared lattice bands of quartz. *Phys. Rev.*, **121**, 1324–1335.

Stull, V. R., P. J. Wyatt and G. N. Plass, 1963: The infrared absorption of carbon dioxide. Aeroneutronic Rept. SSD-TDR-62-127, III, Newport Beach, Calif., 100 pp.

U. S. Standard Atmosphere Supplements, 1966: Prepared by ESSA, NASA, and the U. S. Air Force, Government Printing office.

van de Hulst, H. C., 1957: *Light Scattering by Small Particles*. New York, Wiley, 470 pp.

——, 1963: A new look at multiple scattering. Rept., Institute for Space Studies, NASA, New York, 81 pp.

Wyatt, P. J. V., R. Stull and G. N. Plass, 1962: Infrared absorption of water vapor. Aeronutronic Rept. SSD-TDR-62-127, II, Newport Beach, Calif., 100 pp.

Zander, R., 1968: Additional details on the near-infrared reflectivity of laboratory ice clouds. *J. Geophys. Res.*, **73**, 6581–6584.